Dynamic fracture of disordered viscoelastic solids

P. Heino and K. Kaski
Laboratory of Computational Engineering, Helsinki University of Technology, Miestentie 3, FIN-02150 Espoo, Finland
(Received 13 December 1996; revised manuscript received 6 June 1997)

Dynamic fracture of disordered viscoelastic solids is studied computationally using the Born-Maxwell model. Two types of disorder have been considered, namely, correlated density disorder and topological disorder. In both cases fracture instability in terms of crack branching occurs. For density disorder dense spots in the system are found to be an effective mechanism of crack arrest. This shows in the length of the daughter cracks and also serves as a mechanism for crack curving. In case of topologically disordered systems we see branch bending. The complicated topology of cracks obeys a scaling law which has been found experimentally. [S1063-651X(97)00210-9]

PACS number(s): 62.20.Mk, 61.43.Bn, 83.50.Tq

I. INTRODUCTION

Recently dynamics of fracture has received considerable interest. Experiments [1–4], numerical simulations [5–7], and analytical calculations [8–10] have been performed in order to gain insight into the complicated nature of crack propagation. In the case of amorphous brittle solids experimental results show that a crack propagates with a velocity much below the Rayleigh speed. After reaching a critical value an instability occurs and the crack velocity starts to change in magnitude, or direction or both. Yet these phenomena and the dependence of the system's behavior on the length scale are not well understood [11].

From a microscopic point of view the material is considered as a set of mutually interacting particles (atoms or molecules). A crack propagates, when the distance between two adjacent particles becomes so large, that the interaction between them ceases, i.e., the bond between them breaks. Such an approach is physically correct, but can not be used to study very large systems. However, from the engineering point of view material of macroscopic scale objects is modeled as a continuum. A failure occurs when the maximum stress or some other critical parameter [12] exceeds a given threshold. Some of these criteria are isotropic and cannot explain the easy directions of crack propagation present in molecular-dynamics studies [5]. In addition, in microstructure, many materials are anisotropic, inhomogeneous or disordered, which make continuum approach difficult to model.

Because of these difficulties at both ends of the length scale it makes sense to study fracture in the intermediate, i.e., mesoscopic scale. There the material is considered neither as a continuum, nor as a set of atoms, but rather as a discretized set of interacting mass sites, obtained by dividing the material into regions [13–15].

Apart from the dependence of fracture on the length scale there is also the dependence on the disorder of the material. In this study we consider two types of disorder, namely, topological and correlated. Topological disorder exists in amorphous materials which can be described as random networks with random locations of particles or mass sites. Correlated disorder is found for example in paper as a result of it being a fiber composite.

II. THE BORN-MAXWELL MODEL

In order to describe the dynamic fracture behavior of a disordered system at mesoscopic length scale and under constant rate loading we have chosen a dynamic Maxwell-dissipative model as previously [14,15]. When the system under loading deforms, two (initially) nearest neighbor sites i and j move giving rise to elastic and plastic displacements. The total displacement and elastic displacement of site i are denoted by $\vec{u}_i$ and $\vec{u}_{e,i}$, respectively. In the Born-Maxwell model these sites are connected with springs and dashpots. The spring constants are α_{ij} and β_{ij}, representing tensile and bending stiffness of a bond ij, respectively. The dashpots are parametrized with coefficient τ that describes the rate of plastic deformation phenomenologically.

Let us now denote the elongations of the springs parallel and perpendicular to the unit vector from site i to site j with $\epsilon_{e,ij,\parallel}$ and $\epsilon_{e,ij,\perp}$, respectively. Then the energy of the bond between neighboring sites i and j can be written as [15]

$$H_{ij}=\frac{\alpha}{2}\epsilon_{e,ij,\parallel}^2+\frac{\beta}{2}\epsilon_{e,ij,\perp}^2 . \tag{1}$$

The elongations of the springs are related to the elastic displacements of the sites:

$$\epsilon_{e,ij,\parallel}=\vec{d}_{ij,\parallel}\cdot(\vec{u}_{e,j}-\vec{u}_{e,i}), \tag{2}$$

$$\epsilon_{e,ij,\perp}=\vec{d}_{ij,\perp}\cdot(\vec{u}_{e,j}-\vec{u}_{e,i}), \tag{3}$$

where $\vec{d}_{ij,\parallel}$ is the unit vector of an undeformed bond ij and $\vec{d}_{ij,\perp}$ is a unit vector perpendicular to it, see Fig. 1.

Sites i and j are considered to represent certain pieces of material around them. Their masses, m_i and m_j, depend on the density of the system and on the size of the pieces. Now the equation of motion for a mass site j can be written

$$m_j\ddot{\vec{u}}_j=-\nabla\sum_{i\in nn_j}H_{ij}=\sum_{i\in nn_j}\alpha[(\vec{u}_{e,i}-\vec{u}_{e,j})\cdot\vec{d}_{ij,\parallel}]\vec{d}_{ij,\parallel}+\beta[(\vec{u}_{e,i}-\vec{u}_{e,j})\cdot\vec{d}_{ij,\perp}]\vec{d}_{ij,\perp}, \tag{4}$$

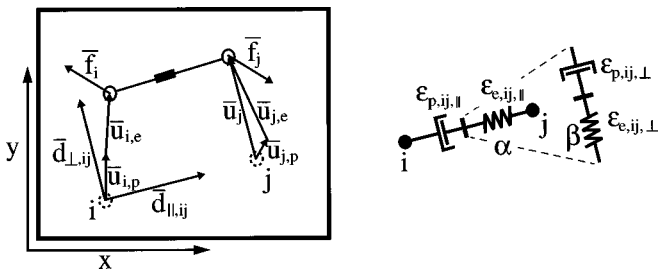

FIG. 1. Description of the model. Two nearest-neighbor sites are connected with dissipative Born-Maxwell springs. The elastic and plastic displacements of the sites results in elongations of the springs and dashpots, respectively. The force due to these springs drives the mass sites.

where nn_j denotes the set of nearest neighbors of site j. As mentioned above plasticity of materials is taken into account as Maxwell-type dashpots, in which the elastic displacements of sites relax according to (see Ref. [15] for details)

$$\dot{\vec{u}}_{e,j}=\dot{\vec{u}}_j-\frac{1}{\tau}\vec{u}_{e,j}. \tag{5}$$

The criterion of local rupture in this model is based on the distance between the neighboring mass sites i and j. When the length of this bond exceeds a given threshold, the bond breaks irreversibly (i.e., $H_{ij}=0$) and a crack propagates across the bond ij.

In the simulations the integration is performed with the original Verlet algorithm [16] by setting the initial conditions $\vec{u}_i=\vec{u}_{e,i}=\vec{0}$ and $\dot{\vec{u}}_i=\vec{0}$. With free vertical boundaries, the bottom row of mass sites is fixed and the loading is realized by moving the topmost row of mass sites. In order to minimize the initial generation of sound waves in the beginning of loading it is introduced in two stages. First for short time interval $0\leqslant t\leqslant T_r$ the loading is increased gradually by moving the topmost row of mass sites with the varying rate $\frac{1}{2}v_s\{1-\cos[\pi(t/T_r)]\}$, and then $(t>T_r)$ keeping the rate constant v_s.

In order to relate our model with macroscale models we next discuss the continuum systems. They are usually solved with the finite element method (FEM) [17,18], obtained by dividing the system into elements. The energetics of each individual element is described by its deformation. In FEM one needs an interpolation scheme for the displacement field within each element. However, when the system is strongly disordered, a correct interpolation scheme is hard, if not impossible to find. In contrast no such interpolation scheme is needed in the case of the Born-Maxwell (BM) model. On the other hand the maximum principal stress of finite element systems is often used as a critical parameter for rupture, i.e., the fracture criterion is isotropic. However, at the mesoscopic or microscopic length scales anisotropy plays a significant role, because there the crack propagation arises from bond failures, the propagation direction being perpendicular to each breaking bond. When a lumped mass approximation [17] is used in FEM, the kinetic energy of the system is a sum of the kinetic energies of nodes (mass is lumped to a node having certain velocity). This is identical with how the kinetic energy is calculated for the Born-Maxwell model. In addition, the potential energy of a regular spring network and the finite element model can be shown to be identical [19]. However, the potential energy of the BM model differs from that of a regular spring network and thus from that of the finite element model.

III. TOPOLOGICAL DISORDER

In the previous section we described how two nearest-neighbor sites interact, but did not specify when two mass sites of a system are considered nearest neighbors. In a regular lattice this is not a problem, and studies have been done both in square and triangular lattices [14,15]. However, the underlying symmetry affects the fracture behavior, since the crack propagates perpendicular to the bonds.

The situation is different in disordered systems. For example, the microstructure of amorphous materials do not resemble any type of lattice. In order to tackle this type of disorder some generic networks topologies have recently been considered [20,21]. Such networks are modified from a regular lattice by randomly moving the sites, but keeping the nearest neighbors the same. In addition to this disorder in microstructure some composite materials, e.g., paper, show disorder in the mesoscopic scale.

Another approach to generate a random network is to randomly select the locations for mass sites [22]. In this case the nearest-neighbor problem can be solved using Voronoi polygons. Given a finite set of points $\vec{p}_k$ the Voronoi polygon of a point $\vec{p}_i$, $\mathsf{L}(\vec{p}_i)$ is defined as the set of points that are closer or equally close to point $\vec{p}_i$ with respect of any other point $\vec{p}_j$:

$$\mathsf{L}(\vec{p}_i)=\{\vec{p}\,|\,d(\vec{p},\vec{p}_i)\leqslant d(\vec{p},\vec{p}_j)\}, \tag{6}$$

where $d(\cdot,\cdot)$ is the distance measure [23]. In our case the Euclidean measure $d(\vec{p}_1,\vec{p}_2)=\sqrt{(\vec{p}_1-\vec{p}_2)\cdot(\vec{p}_1-\vec{p}_2)}$ was used. According to this definition two sites i and j are considered nearest neighbors, if their Voronoi polygons share a common side. If the locations of these sites are selected randomly, it is *highly* improbable that this side reduces to a point, as in square lattices on diagonals.

In Delaunay's triangulation two nearest-neighbor sites of the Voronoi polygon are connected with a straight line. The triangulation can be made fast using sophisticated algorithms such as those described by Macedonio *et al.* or Joe [23,24]. In this way the generated network has neither a symmetry nor an initial lattice that might affect the results. If the bonds in the Born-Maxwell model are considered to represent elastic bars of certain cross-sectional area, the elastic parameters of the bond should be inversely proportional to the initial length of a bond. We have used this interpretation in our simulations. Thus, in practice an initial location for a site is not selected entirely randomly, because two sites should not be too close to each other. Also several mass sites should be on the boundaries for keeping bond lengths reasonably small near the boundaries.

IV. CORRELATED DISORDER

Apart from the disorder in the locations of mass sites it can show in the density, elastic parameters or rupture thresh-

old. In this study the density of the system is considered to be a function of location. This is the case in a sheet of paper as measured by β radiogram or is even visible against light. In earlier studies [25] elastic parameters were considered proportional to density, though recent findings indicate that it is the rupture threshold that controls the fracture process [26]. However, in the latter study the static model consisted of interacting cells and the fracture proceeded by breaking a cell when the plastic strain exceeded a given threshold value. In our model crack propagates, when the distance between two mass sites (which depends on the initial bond length l_0, and plastic and elastic displacements) exceeds a given threshold. This makes the comparison of these two models fairly difficult.

The mass distribution in paper is strongly correlated, i.e., there exists strong elliptic areas called flocs and weak spots. In order to find out the correlation length or size of flocs one can determine it as the half width at half height of the autocorrelation function of the mass distribution [27]. This kind of correlated disorder can be generated by placing elliptical unit mass flocs of given size at random locations on a two-dimensional model sheet [28]. The mass distribution is the result of overlapping flocs. Here we allowed anisotropy in the mass distribution by choosing the principal axis of elliptical flocs to be either in the X or Y direction. The size of these flocs is defined as the length of the principal axis and the aspect ratio of a floc is defined by the length of floc's X axis divided by the length of the floc's Y axis.

V. RESULTS

A. Summary of previous results

In the previous study [15] we concentrated on crack branching due to the dynamics of the system. Crack branching was observed in a system without disorder, where the branches were straight and formed an angle of 15°–33°, depending on the ratio α/β. We also observed oscillations in the crack speed and crack boundary speed beyond a critical velocity. Even though these oscillations were present beyond a critical crack velocity, analysis with the BM model suggested that the crack boundary velocity should determine the conditions for crack branching.

In addition to ordered systems we studied systems, where the elastic constants of the bonds were selected from a uniform distribution, but by keeping the relation $\alpha/\beta=2$ constant [15]. This inclusion of disorder added noise to the branching angles. On the other hand, an inclusion of dissipation was seen to decrease the lengths of daughter cracks.

B. Correlated density distribution

In case of correlated disorder we have studied systems with density variation of 5, 10, and 20 % in a regular triangular lattice, which is comparable with those found in commercial paper grades (typically $\leqslant 10\%$).

A very heterogeneous system can be generated by letting only few flocs to overlap but when the number of flocs is increased, the variation (standard deviation per mean) decreases. For a typical system (system width $=170\times$height$=55$, with floc size 20 and aspect ratio 5), distribution with 20% variation can be generated with $\approx 14\times 10^3$ flocs, while a distribution with 10% variation needs $\approx 55\times 10^3$ flocs and 5% variation is obtained with $\approx 220\times 10^3$ flocs. A typical distribution with 10% variation is shown in Fig. 2.

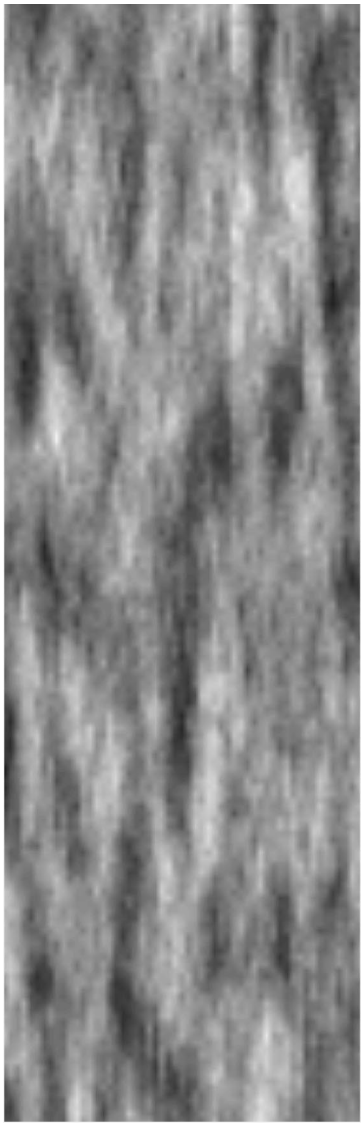

FIG. 2. A typical flocculated density distribution for a system of size 170×55. The system has $\approx 59\times 10^3$ overlapping flocs of size 20×4 and a variation of 10%. Light areas are dense.

As there is no agreement on whether these variations should be reflected in the elastic parameters [25] or the rupture threshold [26], we have studied both types of disorder. The average value for the mass of a site was set to 1, the average elastic parameters were set to $\alpha=500$ and $\beta=250$, the average rupture threshold was set to 1%, the phenomenological dissipation constant was set to $\tau=25$ and the strain rate was set to $v_s=10^{-4}$. (The bond breaks, when its length exceeds $(1+p)l_{0,ij}$, where $l_{0,ij}$ is the initial distance between the mass sites i and j and p is the rupture threshold, whose average is 1%.) In all these systems (of size 170×55) we used flocs of size 20 along the largest direction and the aspect ratios of 5 and 1/5. In the case of large density variation we used flocs of size 10 and 40 along the largest direction and the same aspect ratios. The statistics was taken over 10 runs for each parameter set.

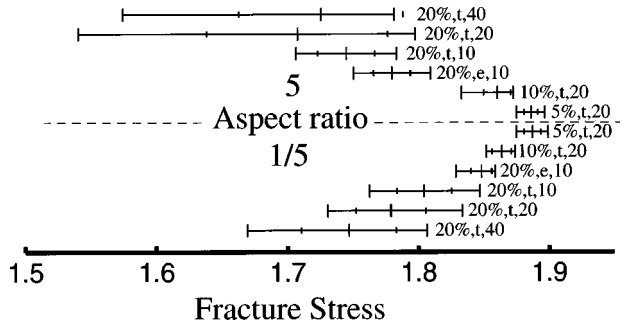

FIG. 3. Fracture stress in different systems with density disorder. Left and right boundary of each bar indicate the minimum and maximum stress for systems with correlated disorder as determined from ten runs. The scatter in the data is approximately 10%, which is expected to be larger than in the case of a static resistor network [29] but sufficiently small for a fully dynamical system, such as ours. The mean and mean $\pm$ standard deviation are also shown. The type of system is denoted by three symbols. The first=5, 10, 20 % indicates variation of the density distribution, the second=e,t corresponds to variations in elastic parameters (e) or the rupture threshold (t). The third=10, 20, 40 is the size of the floc, whose aspect ratio is 5 above the dashed line and 1/5 below it.

We found that the strength of the system, i.e., the rupture stress, increases when disorder of the system decreases (Fig. 3). This is due to the weak spots in the system, where a crack can initiate. If these spots are large enough, the crack can propagate. When the disorder is correlated and the floc size is large enough, the weak spots can be large. This also explains, why systems with small flocs are stronger than systems with large flocs.

We also found that systems with the floc aspect ratio 5 are weaker than systems with floc aspect ratio 1/5. This is due to the flocs near the weak spots in systems with the floc aspect ratio 1/5. These flocs may arrest an already initiated crack and thus prevent it from propagating. In systems with floc aspect ratio 5 also the weak spots are oriented perpendicular to the applied strain, and therefore it is unlikely that a floc could arrest a propagating crack.

The flocs may arrest also a propagating main or daughter cracks. When disorder is small this is not likely to occur, and a crack propagates straight and produces long daughter cracks. However, when the system is more disordered, the flocs are likely to arrest daughter cracks, resulting in only short daughter cracks. When the main crack is arrested by a floc, a daughter crack is likely to propagate through a weak spot and becoming a new main crack. This phenomenon gives rise to crack curving.

Systems in which disorder is reflected in the elastic parameters are found to be stronger than systems, where disorder is in the rupture threshold. In these systems crack arrest is more often seen than in systems, where the disorder is in the rupture threshold. Thus systems with large disorder in the elastic parameters behave quantitatively different from systems with small disorder in the rupture threshold, even if the strength of these systems is the same.

In order to study the finite size scaling behavior of the stress-strain curves we used 11 different system sizes of rectangular shape with width (X direction) being three times the height (Y direction). The largest system we studied consisted of $\approx 2\times 10^5$ mass sites. The density distribution was generated using flocs of size 20 and aspect ratio 5. The fracture stress (σ_f) and fracture strain (ϵ_f) of the system decreases as the size of the system increases and seems to follow the form suggested by Duxbury *et al.* [29]:

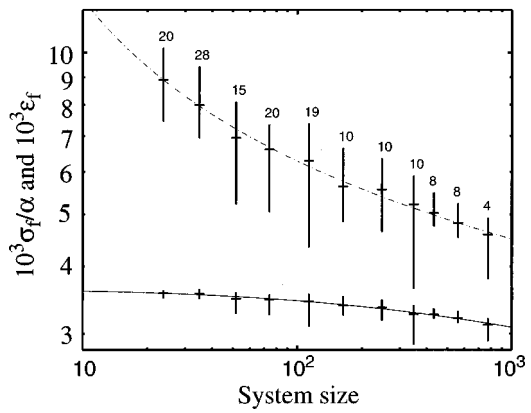

FIG. 4. Fracture stress (σ_f) divided by α (solid line) and fracture strain (ϵ_f, dashed line) as functions of the size of the system (flocculated density disorder). Vertical bars indicate maximum and minimum, horizontal bars indicate the average. Numbers above the bars indicate the number of systems studied. Lines stand for the scaling form of Eq. (7) fitted by the data.

$$\sigma_f = \frac{1}{a + b(\ln L)^c}, \tag{7}$$

where L is the size (i.e., width) of the system, cf. Fig. 4. Studies by Korteoja *et al.* [25] suggested that the fracture stress could have a nonzero value at the thermodynamical limit, which our results do not support. However, in that work a static continuum model was used, which does not resemble the random fuse network model by Duxbury *et al.* [29]. Our model consists of breaking bonds and is therefore closer to the model of Duxbury and thus it is understandable that the scaling behavior of these two models is quite similar.

For fracture strain (ϵ_f) the estimate of the power-law exponent was found to be $c \approx 0.56$, which is also in agreement with the theoretical considerations [29]. However, the fracture stress tends to 0 much faster ($c \approx 3.2$). The reason for this is depicted in Fig. 5, where we show a typical stress vs strain curve for a small system. When the fracture strain decreases by an amount $\Delta\epsilon_{f1}$, the fracture stress decreases by an amount $\Delta\sigma_{f1} \approx \Delta\epsilon_{f1} E(\epsilon_{f1})$, where $E(\epsilon)$ is the effective Young's modulus $\partial\sigma/\partial\epsilon$. Due to the phenomenological dissipation, $E(\epsilon)$ is fairly small for large ϵ (see Fig. 5). When the fracture strain decreases even further by an amount $\Delta\epsilon_{f2}$, the fracture stress decreases by an amount $\Delta\sigma_{f2} \approx \Delta\epsilon_{f2} E(\epsilon_{f2})$. Since in dissipative systems $E(\epsilon_{f2}) > E(\epsilon_{f1})$ the fracture stress tends to zero faster than the fracture strain.

C. Topological disorder

In the case of topological disorder we chose the initial locations of mass sites at random and set the elastic parameter values inversely proportional to the initial lengths of the bonds. In the model only nearest-neighbor interaction is being considered. In Fig. 6 we show the neighbor distribution

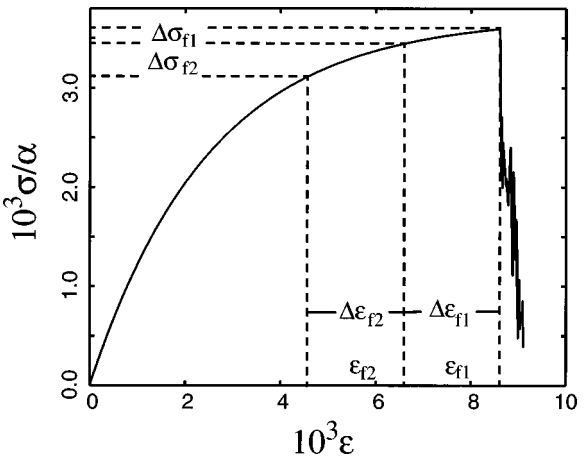

FIG. 5. Stress (σ) vs strain (ϵ) in a small system with correlated density disorder. For small strain the Young's modulus is larger than for large strain. Thus the fracture stress tends to 0 faster than the fracture strain.

of nearest-neighbor mass sites taken from four topologically disordered systems (boundaries excluded). In this figure the lower limit for the bond length, due to the rejection criterion of the random mass site placement procedure, is clearly visible. On the other hand the the upper limit of bond lengths is determined by the density of mass sites. In Fig. 6 we show also the pair-distribution function [30] for distances smaller than roughly 3 times the nearest-neighbor distance. There we see a strong negative correlation, since the existence of short bonds was prohibited. Then at about the nearest neighbor distance there exists a strong positive correlation due to the given density (determined by the number of sites per area) of the system. For long distances we do not see any correlations. In Fig. 6 we also show the distribution of inverse bond lengths, which is comparable to the distribution of elastic constant of the bonds.

In our model the elastic parameters determine the macroscopic features of the system, i.e., the Poisson ratio and the

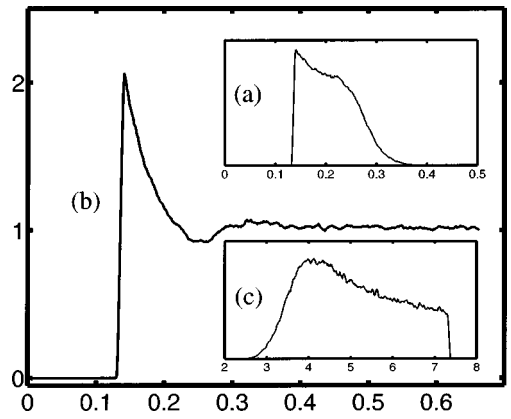

FIG. 6. Bond length (nearest-neighbor distance) distribution (a) and pair-distribution function (b) taken from four topologically disordered systems. For short distances the distribution function is 0, since the existence of such bonds is prohibited by the procedure. Then there is a strong positive correlation at the point determined from the density of sites. For large distances the distribution is uncorrelated. This was checked until the boundary effects became significant, i.e., up to 4.5. The elastic constants were selected proportional to the inverse of bond lengths, distribution (c).

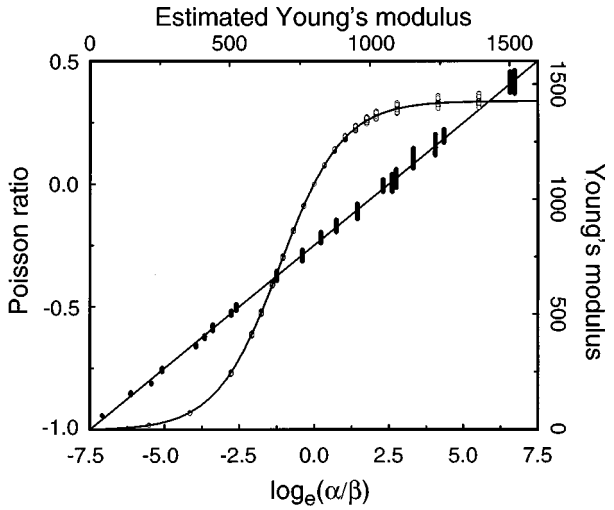

FIG. 7. Poisson ratio vs $\log_e(\alpha/\beta)$ (open circles) of topologically disordered systems and sigmoid function (curved line) fitted to these data. The estimated Young moduli coincides with the true Young moduli reasonably well (black dots and straight line), see text.

Young's modulus. We have calculated these relations from the model by applying the strain of 10% to the system and solving the stable configuration. The dependence of the Poisson ratio on the ratio α/β is depicted in Fig. 7. We found that the deviation in the Poisson ratio was small; all the obtained values (50 topologically disordered systems for a given ratio α/β) are shown in Fig. 7. On a semilogarithmic scale the Poisson ratio ν seems to be of the form of a sigmoid function. It is noteworthy that for $\alpha=\beta$ the Poisson ratio was 0 regardless of the initial configuration. Thus we may require one of the free parameters to be fixed such that the Poisson ratio is zero for $\alpha=\beta$. As the sigmoid function is exponential and has $\ln(\alpha/\beta)$ as an argument, the Poisson ratio can be given in a simpler form:

$$\nu = 3.90\left(\frac{1}{2.91+(\alpha/\beta)^{-0.98}} - \frac{1}{2.91+1}\right). \tag{8}$$

In topologically disordered systems the elastic parameters α_{ij} and β_{ij} were chosen inversely proportional to the initial length of the bond. In the following α and β denote the average of these parameters. The Young's modulus should be of the same order as α and β and go to zero as both α and β go to 0. Thus we were led to try an estimate of the form

$$E = a\alpha + b\beta + c\alpha^d\beta^{1-d}. \tag{9}$$

For numerical stability d should not be either 0 or 1. In fact, this function could predict the macroscopic Young's modulus remarkably well. The fitting factor a was found to be extremely close to 1. With the restriction $a=1$ the correction parameters were $b\approx 0.24$, $c\approx 0.47$, and $d\approx 0.59$. In Fig. 7 the macroscopic Young's modulus is plotted versus its estimate. The density of the bonds does not affect the Young's modulus, since the mean of the elastic parameters is given, and the locations for the bonds are random. In addition, the Young's modulus seems not to depend on the shape of the system.

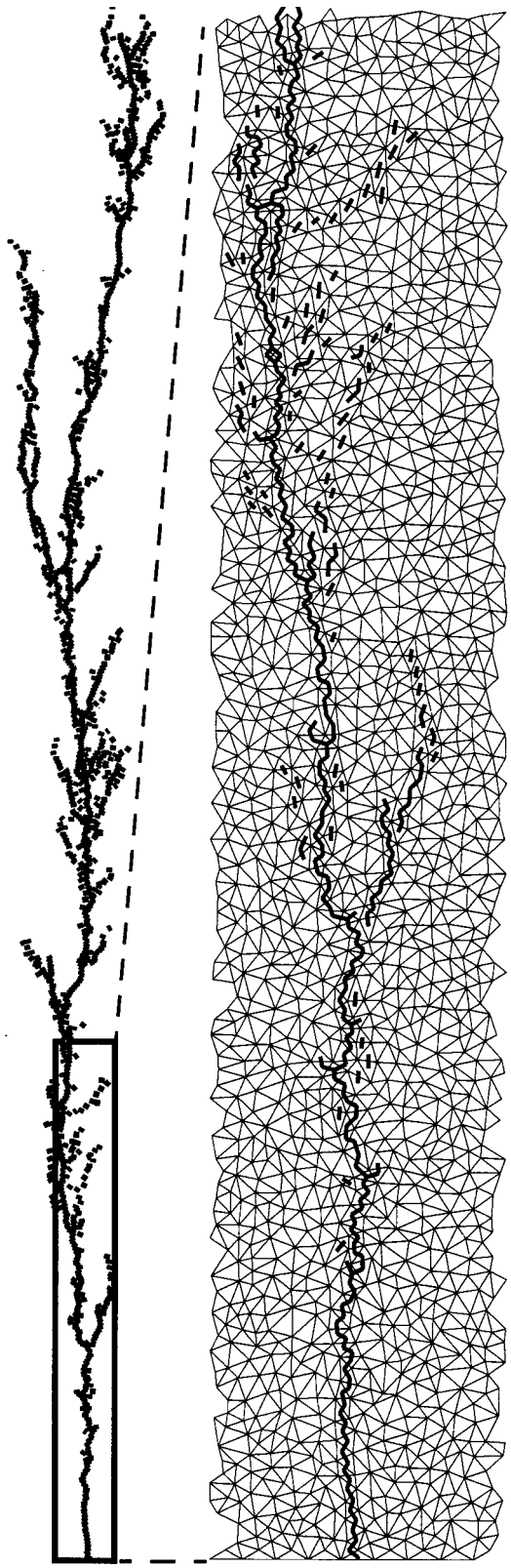

FIG. 8. Typical fracture path obtained from a topologically disordered system. The triangulation of 1/9 of the system and crack propagation in it are presented below the path.

In the simulation of dynamic fracture the elastic parameters were chosen to be on average $\alpha=500$ and $\beta=250$, which corresponds to the Poisson ratio $\nu=0.1$. The mass of a site was set to one third of the mass of triangles surrounding it. Before loading, a cut was introduced to the left free boundary of the system to serve as a seed for crack propagation. The length of this cut was 5% of the width of the system.

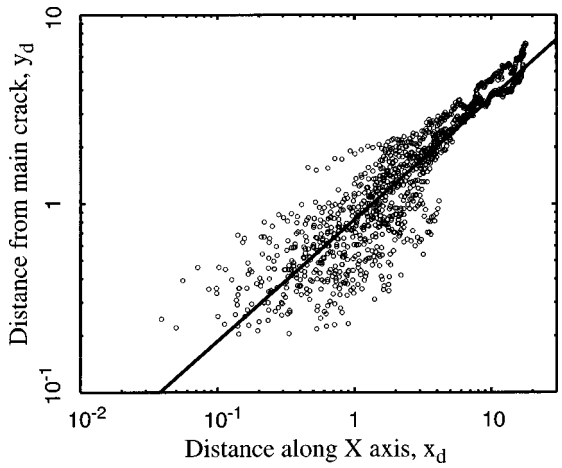

FIG. 9. Daughter crack's distance from the main crack vs daughter crack's distance along the X axis in a topologically disordered system and power-law fit to these data. Long daughter cracks have a branching angle of 15°.

A typical fracture path is presented in Fig. 8. It shows a relatively straight path in the beginning of propagation and a complicated, branched form later. The daughter cracks are seen to curve during propagation such that the branching angle depends on the length of the daughter crack. This is illustrated in Fig. 9, where we show the daughter crack's distance from the main crack as a function of the length of the daughter crack along the X axis. The data obeys roughly a power law: $y_d=ax_d^b$. For small x_d the distance from the main crack is not of functional form, since these small branches are probably responsible for the mist behavior of the fracture surface. For larger x_d the given functional form is clearly seen and these large branches are seen as the hackle behavior. It is quite subjective to determine, which cut bonds belong to the mist region and which are classified as branches. Here the bonds not on the main crack are treated

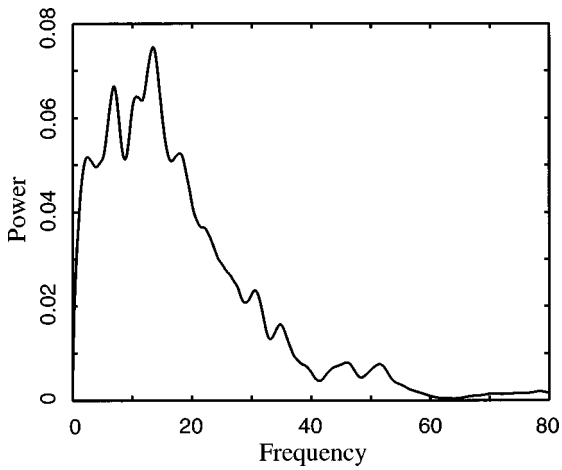

FIG. 10. Spectrum of crack speed in topologically disordered systems obtained as an average of four runs. It shows that crack speed does not fluctuate randomly.

as branches, and therefore the extremely short branches complicate the curving behavior. The power-law exponent b was found to be 0.65 ± 0.02. This is in good agreement with the experimental value 0.7 [1]. We also found that the longest daughter cracks appear with an angle of about 15°, which is in excellent agreement with experiments in brittle amorphous materials [31].

In the unstable region of dynamic fracture the crack speed changes both in magnitude and direction. Sharon and Fineberg [1] have found experimental evidence that these changes are oscillatory rather than random fluctuations. In addition, Blumenfeld [11] by using the Yoffe solution [32] has shown theoretically that the crack speed is oscillatory. Also when noise was added the situation became more complicated showing intermittency and quasiperiodicity. Our Born-Maxwell model with no disorder shows clear oscillatory behavior but in the case of topological disorder the model produces a behavior which is characterized with a fairly wide power spectrum of the crack speed, see Fig. 10.

VI. SUMMARY

A dynamical dissipative model was used to study fracture in systems with two types of disorder. First we studied correlated mass density variation, which resulted in similar variations in either the elastic parameters or the fracture threshold. Results also show similar finite size scaling in the strength of the system as proposed by Duxbury *et al.* [29]. The flocculated density variations are seen as a mechanism for crack arrest. As a second type of disorder we studied systems, in which the initial locations for mass sites were selected randomly. We showed, how to select the elastic parameters for a given Poisson ratio and Young's modulus. Crack speed oscillation was seen as well as daughter crack curving. The experimentally found scaling behavior of crack curving was confirmed.

ACKNOWLEDGMENTS

This work is funded by the Academy of Finland through the Material Physics graduate school and MATRA grant.

[1] E. Sharon, S.P. Gross, and J. Fineberg, Phys. Rev. Lett. **74**, 5096 (1995); **76,** 2117 (1996).
[2] J. Fineberg, S.P. Gross, M. Marder, and H.L. Swinney, Phys. Rev. B **45**, 5146 (1992); Phys. Rev. Lett. **67**, 457 (1991).
[3] S.P. Gross, J. Fineberg, M. Marder, W.D. McCormick, and H.L. Swinney, Phys. Rev. Lett. **71**, 3162 (1993).
[4] A. Yuse and M. Sano, Nature (London) **362**, 329 (1993); M. Marder, *ibid.* **362**, 295 (1993); Ronsin, O. Heslot, and B. Perrin, Phys. Rev. Lett. **75**, 2352 (1995).
[5] F.F. Abraham, D. Brodbeck, R.A. Rafey, and W.E. Rudge, Phys. Rev. Lett. **73**, 272 (1994); F.F. Abraham, *ibid.* **77**, 869 (1996).
[6] M. Marder and X. Liu, Phys. Rev. Lett. **71**, 2417 (1993).
[7] H. Furukawa, Prog. Theor. Phys. **90**, 949 (1993).
[8] K. Runde, Phys. Rev. E **49**, 2597 (1994).
[9] J.S. Langer, Phys. Rev. Lett. **70**, 3592 (1993).
[10] M. Adda-Bedia and M. Ben Amar, Phys. Rev. Lett. **76**, 1497 (1996).
[11] R. Blumenfeld, Phys. Rev. Lett. **76**, 3703 (1996).
[12] F.L. Singer, *Strength of Materials*, 2nd ed. (Harper & Row, New York, 1963).
[13] Y. Mori, K. Kaneko, and M. Wadati, J. Phys. Soc. Jpn. **50**, 1591 (1990).
[14] T. T. Rautiainen, M. J. Alava, and K. Kaski, Phys. Rev. E **51**, R2727 (1995).
[15] P. Heino and K. Kaski, Phys. Rev. B **54**, 6150 (1996).
[16] M.P. Allen and D.J. Tildesley, *Computer Simulation of Liquids* (Oxford University Press, Oxford, 1987).
[17] O.C. Zienkiewicz and R.L. Taylor, *The Finite Element Method*, 4th ed. (McGraw-Hill, New York, 1994).
[18] S.J.D. Cox and L. Paterson, Phys. Rev. B **40**, 4690 (1989).
[19] W.T. Ashurst and W.G. Hoover, Phys. Rev. B **14**, 1465 (1976).
[20] C. Moukarzel and P.M. Duxbury, Phys. Rev. Lett. **75**, 4055 (1995).
[21] D.J. Jacobs and M.F. Thorpe, Phys. Rev. Lett. **75**, 4051 (1995).
[22] A.V. Potapov, M.A. Hopkins, and C.S. Campbell, Int. J. Mod. Phys. C **6**, 371 (1995); **6,** 399 (1995).
[23] G. Macedonio and M.T. Pareschi, Comput. Geosci. **17**, 859 (1991).
[24] B. Joe, Adv. Eng. Softw. **13**, 325 (1991); see also GEOMPACK at URL ftp://ftp.cs.ualberta.ca/pub/geompack or http://www.scs.carleton.ca/~csgs/resources/cg.html This software was used and Joe's implementation is greatly acknowledged.
[25] M. Korteoja, A. Lukkarinen, K. Kaski, and K. Niskanen, Phys. Rev. E **51**, 1055 (1995).
[26] L. Salminen, M. Korteoja, M. Alava, and K. Niskanen, Paperin lujuuden vaihtelusta, KCL Paper Science Centre Communications 89 (1996). (In Finnish, to appear in English, ISSN 0786-9924.)
[27] M. Korteoja, K. Niskanen, K. Kaski, and M.T. Kortschot, *Progressive Damage in Paper*, Helsinki University of Technology report, 1997 (unpublished).
[28] M. Korteoja, A. Lukkarinen, K. Niskanen, and K. Kaski, *Proceedings of the International Paper Physics Conference*, Niagara, 1995 (unpublished) (see also the work by R.R. Farnood and C.T.J. Dodson therein).
[29] P.M. Duxbury, P.L. Leath, and P.D. Beale, Phys. Rev. B **36**, 367 (1987).
[30] A. Rahman, Phys. Rev. **136**, A405 (1964).
[31] E. Sharon and J. Fineberg, Phys. Rev. B **54**, 7128 (1996).
[32] E.H. Yoffe, Philos. Mag. **42**, 739 (1951).